United States Department of the Interior
BUREAU OF RECLAMATION
DENVER OFFICE
P O BOX 25007
BUILDING 67, DENVER FEDERAL CENTER
DENVER, COLORADO 80225-0007

IN REPLY
REFER TO:
D-3744

MEMORANDUM

To: Head, Remote Sensing and Geographic Information Section
Attention: D-3744

From: David W. Eckhardt, Physical Scientist

Subject: Mapping Water Quality on Lake Powell Using Landsat Thematic Mapper Imagery (Remote Sensing)

Applied Sciences Referral Memorandum No. 94-4-1.

INTRODUCTION

Lake Powell began forming when the diversion tunnels around Glen Canyon Dam were closed in 1963. When Lake Powell filled in June of 1980, it became the largest reservoir in the Colorado River system, with a storage capacity of over 27 million acre-feet (33.3 billion m^3). Lake Powell is located on the Colorado River in arid northern Arizona and southeast Utah (figure 1). The Colorado and San Juan Rivers contribute over 95 percent of the lake's annual inflow (Stockton and Jacoby, 1976). For the most part, the flow of these rivers comes from snowmelt in the Rocky Mountains of Colorado, Wyoming, Utah, and New Mexico. Runoff peaks in May and June, and is at its minimum in January (ReMillard et al., 1992). The lake was created primarily to guarantee legally mandated river flows from the Upper Colorado River Basin states of Utah, Wyoming, Colorado, and New Mexico, to the Lower Colorado River states of Arizona, Nevada, and California in times of drought. In addition, Lake Powell serves as a popular recreation area, recording almost 2.5 million visitor days each year (Potter and Drake, 1989). The turbines in Glen Canyon Dam produce approximately 4 billion kilowatt hours of hydropower each year (U.S. Bureau of Reclamation, 1990).

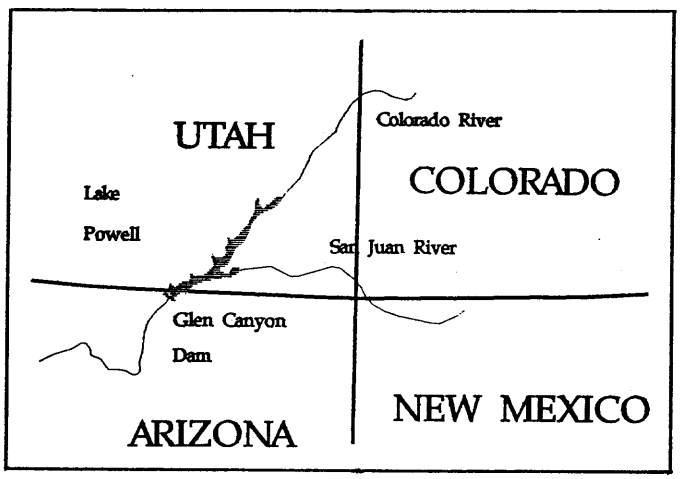

Figure 1. Lake Powell is located along the Colorado River in northeast Arizona and southeast Utah.

452.05
L192
10079
NMP4576
T2

As part of an ongoing program to monitor the effects of Glen Canyon Dam and Lake Powell on the Grand Canyon downstream, water quality in Lake Powell is routinely monitored by Reclamation's Glen Canyon Environmental Studies office in Flagstaff, Arizona. Current monitoring is based solely on point sample data. Extrapolating these data to unsampled parts of the lake is uncertain and totally dependent on analyst knowledge of the reservoir. Numerous researchers have developed models that predict water quality parameters from Landsat MSS (Multispectral Scanner) and TM (Thematic Mapper) image grey values (Verdin and Wegner, 1983; Lathrop and Lillesand, 1986, 1987; Lira et al., 1992). These models are applied to the entire water body, generating maps of water quality parameters from a limited set of point sample data. These models are affected by a multitude of environmental factors; and increased limnological complexity frequently reduces prediction accuracy. This project was funded to determine if Landsat TM imagery could be used to reliably extrapolate point-sampled water quality data on limnologically complex Lake Powell.

This paper describes how a multispectral Landsat TM image acquired on October 14, 1992 was used to successfully map chlorophyll-a concentration, Secchi depth, and surface water temperature on Lake Powell. The methods described here are useful for mapping water quality in other large reservoirs and lakes. The resulting maps give a 2-dimensional view of water quality parameters that is not available from any other source. These maps offer new perspectives to limnologists studying the physical and biological dynamics of Lake Powell.

COLLECTING AND PREPARING FIELD AND IMAGE DATA

On 10/14/92, five sampling teams measured water quality parameters at 110 sites on Lake Powell. The location of each sampling site was determined using GPS receivers. The Landsat TM image acquired the same day was preprocessed to reduce systematic and random noise, and a coordinate transformation equation was calculated to relate geographic coordinates to image row/column coordinates. Finally, image grey values were extracted from the image at the calculated sampling site coordinates and merged with the sampled water quality measurements. The models which predict water quality from image grey values were derived from this data set.

Collecting Water Quality Samples

Lake Sampling

Five teams sampled Lake Powell on October 14, 1992, the day of the Landsat 5 overpass. The five teams collected samples at a total of 110 stations distributed throughout Lake Powell (figure 2). At each station, sampling crews measured surface water temperature, conductivity, dissolved oxygen, and Secchi depth. In addition, crews collected surface and composite 0-5 meter water samples from which chlorophyll-a concentrations were derived. The surface samples were collected by hand in a one-liter bottle. The composite samples were collected by:

1) slowly lowering a weighted 5-cm diameter swimming pool hose to a depth of 5 meters,
2) plugging the end of the hose in the boat with a rubber stopper, thereby trapping the column of water in the hose,
3) raising the hose into the boat using a rope attached to the weighted end of the hose,
4) removing the rubber stopper and transferring the water from the hose into a bucket, and
5) drawing a one-liter sample from the bucket.

These samples were stored on ice in the dark until they could be processed using standardized methods to determine chlorophyll-a concentration

(Strickland and Parsons, 1968).

Sampling crews noted the starting and ending times of sampling, as well as environmental observations such as cloud cover percentage and type, wind speed

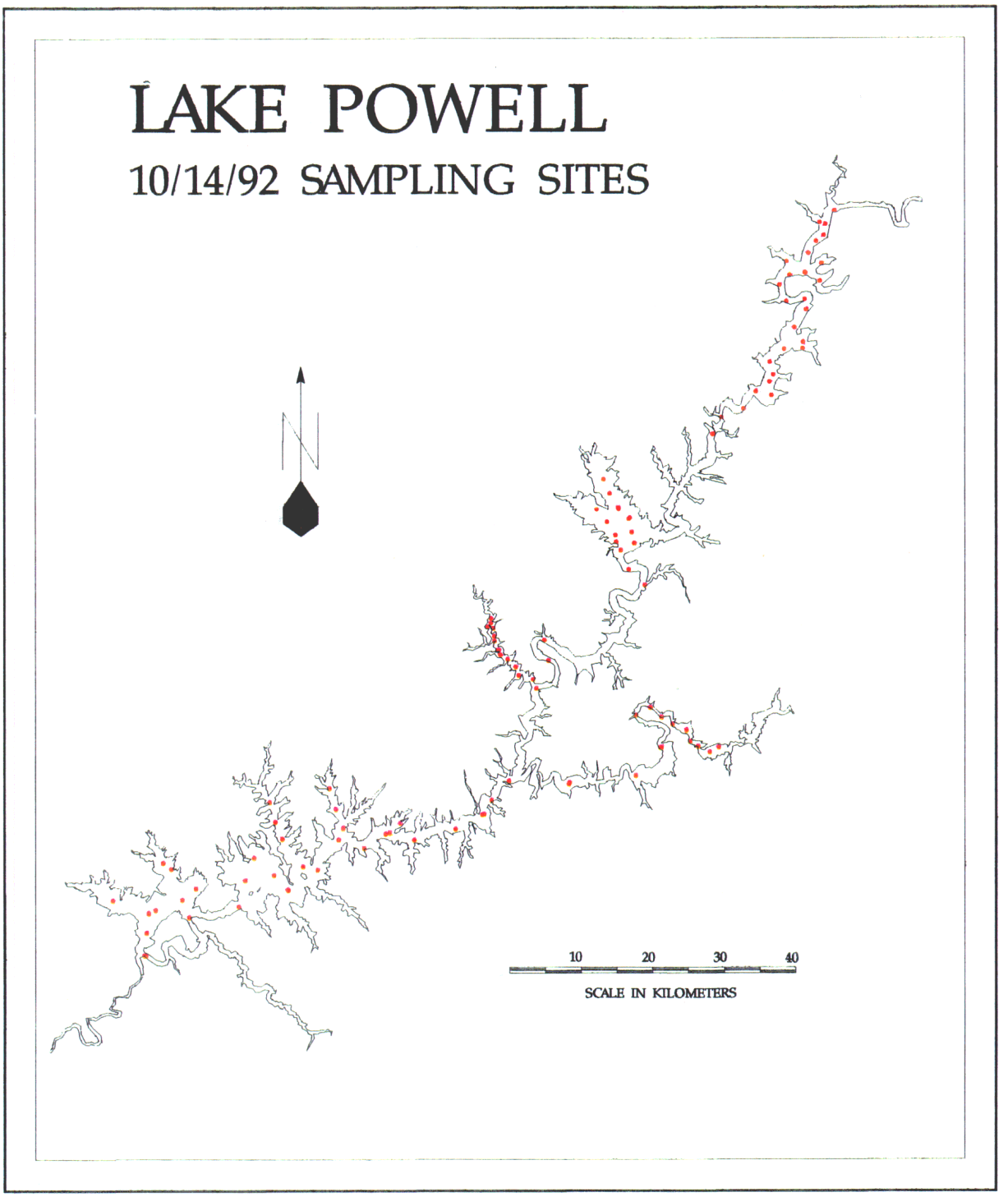

Figure 2. Locations at which samples were collected on October 14, 1992.

and direction, and wave height. Miscellaneous notes were also recorded that were useful when the sampled data were analyzed with the image data, e.g. "river is plunging here", or "woody debris on the surface of the water".

Determining Locations of Sampling Boats

GPS (Global Positioning System) receivers recorded the geographic coordinates of the sampling boats at each sampling site. GPS receivers use precise signals from a constellation of DoD (Department of Defense) navigation satellites to determine geographic position anywhere in the world. Signals from four satellites are required for a 3-dimensional fix (latitude, longitude, and elevation), while signals from three satellites are adequate to determine latitude and longitude, if elevation is known. GPS receivers were used because they compute accurate position fixes in real time, at all times of day, and under all weather conditions.

C/A (coarse acquisition) code GPS receivers were used for this study. These receivers calculate a new position about once per second. Coordinates for each sampling site were stored as a separate file in an electronic data logger. Under optimum conditions, the positional accuracy of fixes from C/A code GPS receivers is typically 20 to 30 meters. However, during the sampling of Lake Powell, DoD was operating the constellation of GPS satellites under S/A (Selective Availability). S/A is the intentional degrading of GPS signals to limit their usefulness to a potential military adversary. The magnitude of S/A positional error varies with time, but it can be 100 meters or more. Fortunately, the errors introduced with S/A, as well as others introduced by atmospheric delays of the GPS signals, can be drastically reduced by post-processing using data from a GPS base station. A base station is another GPS unit which collects data at a known location simultaneous to the "roving" GPS units. Post-processed individual GPS positions typically have accuracies of 5 to 10 meters. For this work, a base station was operated at the National Park Service warehouse at Wahweap Marina during lake sampling.

Errors in GPS position measurements tend to be normally distributed, so averaging multiple GPS positions increases accuracy (Langley, 1991). Averaging 180 or so GPS positions typically reduces error from 5 to 10 meters to 1 to 3 meters. For this reason, the sampling teams collected a minimum of 180 points (or the maximum number the available memory in their GPS unit would allow) at each sampling site. In many cases, the GPS units were simply turned on when the sampling site was reached, and turned off just before leaving for the next sampling site.

Differential correction was performed on all but 6 of the 110 rover GPS files. The six that could not be differentially corrected were collected when the base station was not in operation. Because all six of the uncorrected GPS positions fell in homogeneous regions of the lake, any S/A-induced position error was deemed to be insignificant. Moving the estimated sample location 100 meters in any direction did not appreciably alter the image grey values in any band.

Differentially corrected GPS positions for each sampling site were plotted in 2-D (two dimensions) and inspected to see if the GPS data were tightly grouped, or if the distribution appeared to be fragmented with groups of outliers separate from the main data distribution. Outliers were present at 23 sites. The outliers at all 23 sites had been calculated in 2-D mode (using three satellites instead of four to calculate a position). Large errors for positions calculated in 2-D mode are the result of the GPS unit using its last autonomously-computed elevation estimate and signals from only three satellites to calculate latitude and longitude. Due to the geometric configuration of the GPS satellite constellation, the elevation component of a GPS position contains at least 1.5 times as much error as the horizontal

component, which itself can be over 100 meters in the presence of S/A. When such an error-prone estimate is used in the calculation of horizontal position, horizontal accuracy suffers. 2-D positions acquired on 10/14/92 were improved by manually resetting the elevation of each point to its actual value, and recalculating the position. Any adjusted 2-D positions that were still major outliers were removed from their data set.

The edited GPS data sets were then averaged to yield the best estimates of sampling boat positions. Unfortunately, boat drift was severe (over 100 meters) for about 30-percent of all sampling sites. Because sampling teams did not record the exact times at which they sampled, the sample positions could be in error by up to half of the drift distance. This positional error usually did not cause any problems due to the spatial homogeneity of much of the lake. However, in areas of high spatial variability, the locational uncertainty led to dropping several samples from consideration when developing water quality prediction models.

Preparing the Image Data

Thematic Mapper Imagery

The TM sensor is carried aboard the Landsat 4 and Landsat 5 satellites (figure 3). These satellites orbit the earth at an altitude of 705 km, and have an orbital revisit cycle of 16 days. TM produces imagery in a 185 km-wide swath in seven different wavelength bands. TM1 (TM band 1) through TM4 are in the visible and near IR (infrared) part of the spectrum, TM5 and TM7 are in the middle IR region, and TM6 is in the thermal IR region (table 1). Ground-projected pixel size is 30 meters for TM1-TM5 and TM7, and 120 meters for TM6; but the standard geometrically corrected TM image product has all bands resampled to a 28.5 meter pixel size. All bands are quantized to 8-bits (256 possible grey levels).

Image Preprocessing

The TM sensor was designed for terrestrial applications. Because water bodies are among the darkest objects in any TM scene, image brightness variations within water bodies typically occupy only a small fraction of the total dynamic range available to the TM sensor. The low reflectance of water bodies makes them more susceptible to degradation by the systematic and random noise found in all TM images. For this reason, extra care was taken to reduce TM image noise prior to analysis.

The image preprocessing procedures used to prepare the TM data for analysis are described below. These procedures were time-consuming and computationally intensive, but they were necessary to increase the utility of TM data for water quality mapping.

Excluding Land Area from Processing

The first preprocessing step was to create an image mask that distinguishes water pixels from land pixels. A threshold TM4 grey value was selected which identified all but the most turbid water. For the 10/14/92 Lake Powell scene, pixels with a TM4 grey value of 18 or less were identified as water and assigned a value of 255. The rest of the pixels were identified as land and received a value of zero. This was only a preliminary land/water mask because all land pixels in shadow were identified as "water", and pixels containing extremely turbid water, large boats, and large airplanes were identified as "land". The image analyst visually identified the areas containing these kinds of errors, and used image processing procedures to correct the image

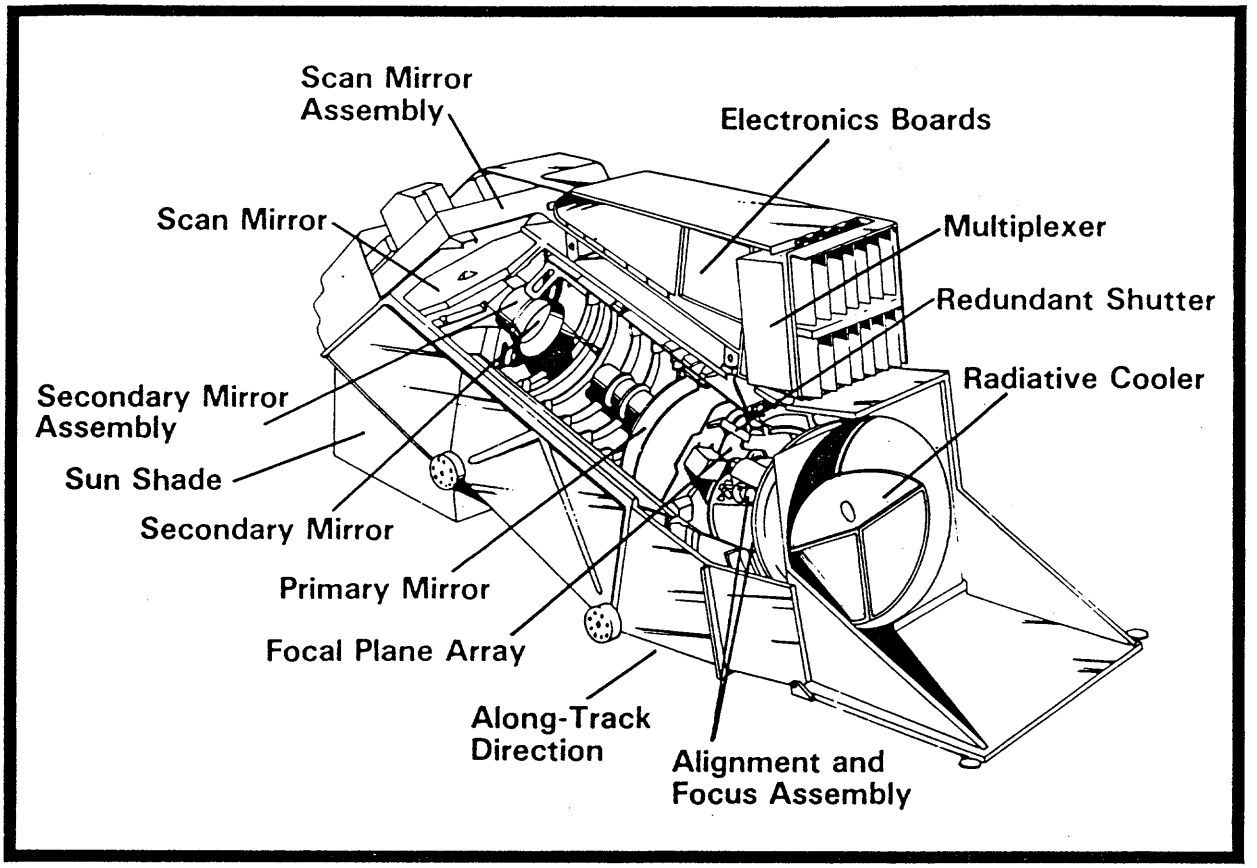

Figure 3. The Landsat Thematic Mapper Sensor. A scanning mirror and optics direct light from the earth onto an array of sensitive light detectors. Here, light intensity in several different wavelength bands is measured and quantized for each 30- by 30-meter area (for TM1-5 and TM7) or 120- by 120-meter area (for TM6) on the earth's surface. These digitized brightness values are then transmitted to earth, where they are reconstructed into digital images.

TM Band	Spectral Range (micrometers)	Description
1	0.45 - 0.52	blue
2	0.52 - 0.60	green
3	0.63 - 0.69	red
4	0.76 - 0.90	near infrared
5	1.55 - 1.75	middle infrared
7	2.08 - 2.35	middle infrared
6	10.40 - 12.50	thermal infrared

Table 1. Landsat Thematic Mapper Spectral Bands.

mask grey values in the identified areas.

To minimize manual editing, the TM4 water identification threshold was set to a value that is considerably higher than that of the average pure water pixel.

As a result, numerous pixels along the edge of the lake were identified as "water", when in fact they are slightly contaminated with reflectance from the adjacent land. To exclude these pixels from the land/water mask, a 3x3 minimum filter was passed over the edited preliminary water mask to move the land/water boundary inward one pixel in all directions. This mask is referred to as the LAKEONLY mask.

The 120-meter pixel size of TM6 prior to resampling to 28.5 meters means that the effects of land brightness can be observed up to 120-meters from shore. For this reason, a 5x5 minimum filter was passed over the LAKEONLY mask to move the land/water boundary inward an additional two pixels. This mask is referred to as the LAKEONLY6 mask.

Each of the seven TM bands was masked such that only lake pixels remained in a zero background. This masking was accomplished by performing a bitwise logical AND operation with the LAKEONLY and LAKEONLY6 image masks and the raw TM data.

Replacing Pixels Containing Non-water Reflectance

Some pixels identified as water contained some non-water reflectance contamination from boats, boat wakes, airplanes, vapor trails, etc. The image analyst manually identified these pixels within polygons, deleted the image data within those polygons, and then filled the polygons with the average value of their neighboring "water" pixels.

Reducing Image Banding

All TM images contain a systematic horizontal banding noise pattern. This pattern is additive in nature and is present throughout images, but is most noticeable in areas of low reflectance (Helder et al., 1992). Quick transitions from extremely bright to low reflectance targets can produce temporary banding due to detector saturation and sensitivity loss, but the most common banding pattern visible in all TM images is caused by differences in sensor calibration offsets between forward and reverse scans. Each scan images 16 rows of pixels, so the banding pattern within raw TM images has a period of 32 rows. This effect is not correlated with the image and may produce scan differences of up to four grey values (Barker, 1985).

A technique developed by Crippen (1989) was used to remove scan line noise from TM images. The general concept is to subtract scan line noise after it has been isolated by a combination of spatial filters. Crippen's process is outlined below.

1) Apply a 51-column by 1-row low-pass (mean) filter to the image.

   This low-pass filtering removes high spatial frequency information along the image rows, leaving an image with even more easily identifiable banding patterns.

2) Apply a 33-row by 1-column high-pass filter (central pixel value minus filter-window mean) to the output from step 1.

   This column-oriented high-pass filter identifies the banding pattern between scan swaths. A 33-row instead of a 32-row high pass filter is used here because of the difference in pixel size between the standard geometrically corrected TM image product and the raw imagery (28.5 meters compared to 30 meters).

3) Apply a 21-column by 1-row low-pass (mean) filter to the output from

step 2.

This filter suppresses artifacts created by the high-pass filter in step 2, and creates the "banding estimate" image.

4) Subtract the banding estimate image produced in steps 1, 2, and 3 from the original image to create the debanded image.

Crippen's technique is suitable for improving the visual interpretability of most TM images, but is unsuitable if the imagery is to be used for quantitative analyses of water bodies. The main reason for this unsuitability is that near-shore lake pixels can acquire false patterns that are the inverse of high-contrast patters located nearby on the same image row. For example, a high contrast shoreline in a "U" shape will cause the technique to produce anomalous grey values for near-shore pixels near the base of the "U" as extreme differences between adjacent low-pass filtered rows (step 1) generate anomalously high banding estimates (step 2), which, when subtracted from the raw data, produce extreme grey values (step 4).

To make Crippen's technique usable for limnological applications, debanding estimates were calculated from "water" pixels only. Furthermore, all water pixels that are significantly brighter than their neighbors were removed prior to calculating debanding correction factors. A modified version of the LAKEONLY6 image mask was used to exclude high contrast targets in each TM band. The LAKEONLY6 mask not only excludes all land pixels, but it also excludes the 3 lake pixels closest to shore. These near-shore pixels sometimes exhibit enough contrast with nearby lake pixels to cause artifacting in the debanding process. The LAKEONLY6 mask was modified to exclude high contrast areas where extremely turbid water abruptly transitioned to clear water. What is "extremely turbid", however, varies with wavelength. TM1-4 are much more sensitive to turbidity in water than TM5 and 7; while TM6 is completely unaffected by turbidity. For this reason, TM6 used the unmodified LAKEONLY6 mask, while different modifications were performed on the LAKEONLY6 mask for use with TM1-4, and TM5 and TM7.

The above modification to Crippen's debanding technique removed the artifacting problems associated with high-contrast targets. However, excluding land and near-shore pixels dramatically reduced the number of pixels available to define banding patterns. Pixels that did not have 16 "water" pixels above and below them could not be corrected. The number of pixels affected by this limitation was quite large because of the sinuous, narrow shape of Lake Powell.

To increase the number of pixels for which debanding estimates were available, banding estimate values (from step 3) were extended 150 pixels along each row to generate a final banding estimate image. This extension was accomplished through a series of 1-row by multiple-column low-pass (mean) filters which replaced zero background values with averages of the banding estimate pixel values within the filter kernel. Extending banding estimates allowed most pixels whose position in the image prohibited a direct calculation of the estimate to use the average of estimates calculated for neighboring pixels along the same line. Although this technique increased the number of pixels that could be corrected, a small percentage of pixels could not be corrected by virtue of their position in the image.

The final banding estimate image for TM1-5 and TM7 was subtracted from the raw LAKEONLY images so that most lake pixels, even those within 3 pixels of shore and those within extremely turbid areas excluded earlier, were debanded. The TM6 debanding estimate image was subtracted from the raw LAKEONLY6 image. All images created during the debanding process were stored in real (4 bytes per pixel) format, instead of being converted back to byte format. Converting

back to byte can sometimes accentuate any residual banding pattern.

The debanding procedure produced an image whose appearance and utility for quantitative modelling was vastly improved. Furthermore, it did not alter the mean value of any band. The effectiveness of the debanding procedure is illustrated in figure 4.

Reducing Random Image Noise

All TM images contain high frequency "salt and pepper" random noise that is not removed by the debanding procedure. This noise is not correlated with the image data, and exhibits no spatial pattern. Salt and pepper noise was reduced by applying a moving average (mean) filter to the image. Mean filters have the beneficial effect of increasing the signal-to-noise ratio by a factor of the square root of the number of pixels in the filter (Lindell et al., 1986). On the other hand, mean filters reduce the effective spatial resolution of the data, possibly obscuring some detailed patterns that might be visible in the unfiltered data. Four kernel sizes were evaluated for use with the debanded reflective bands (TM1-5 and TM7) of the 10/14/92 Lake Powell TM scene: 3x3, 5x5, 7x7, and 11x11. Images filtered with the 5x5 kernel exhibited the best correlation with chlorophyll-a concentration and Secchi depth, and retained most of the detailed patterns visible in the original image.

For TM6, the thermal band, a 13-row by 13-column mean filter was used to reduce image noise. The 13x13 kernel operating on 28.5-meter TM6 pixels mimics a 3x3 kernel operating on the 120-meter pixels of the raw data. This kernel size effectively reduced image noise without excessively smoothing the data.

Preparing the Water Quality/TM Data Set

Transforming Coordinates

The first step in this process was to identify GCPs (ground control points) on both the TM image and georeferenced map products (maps or orthophoto quadrangles). GCPs are features that are clearly identifiable on both the image and map products, and are used to define the relationship between two coordinate systems. An analyst marked GCPs with pin holes on the map products, and then recorded the image coordinates of the same features to subpixel accuracy.

The differentially corrected GPS coordinates for each sampling site were converted from WGS84 latitude/longitude to NAD27 UTM (Universal Transverse Mercator) northings and eastings. These UTM coordinates were converted to image coordinates using a transformation equation developed from the paired GCP coordinates. The Arc/Info geographic information system was used to perform the coordinate transformation. GCP locations were digitized from orthophoto quadrangles as tics into an ARC coverage in UTM coordinates. The GPS-derived UTM coordinates of the sampling sites were also entered into this coverage as point features using the GENERATE command. The image coordinates of the GCPs were entered as tics into a second coverage using GENERATE. The TRANSFORM command then converted the UTM sampling site coordinates from the first coverage to image coordinates, and stored these transformed coordinates in the second coverage. This conversion was defined by a first-order transformation equation relating the GCP (tic) coordinates from the two coverages.

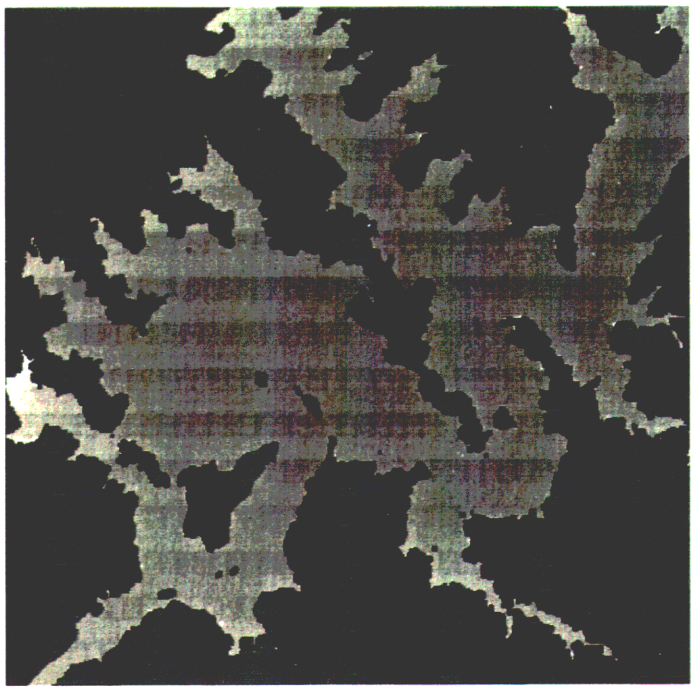

Figure 4a.

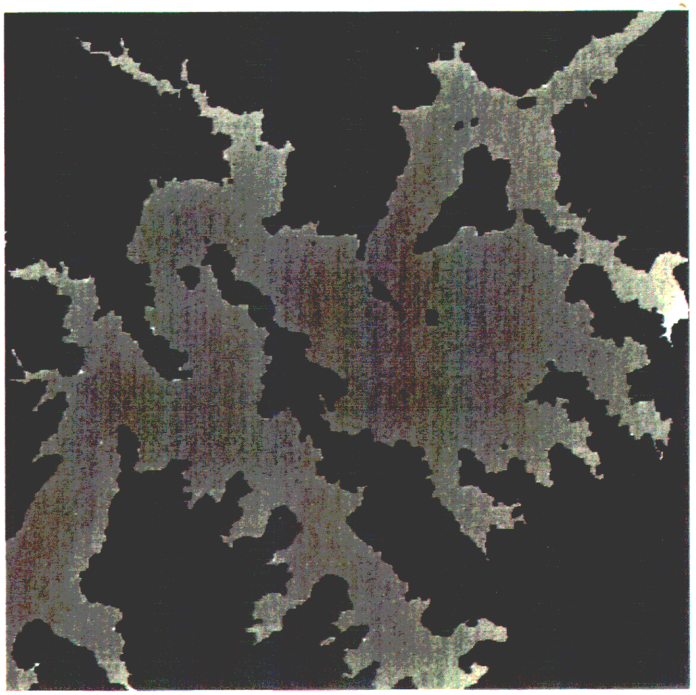

Figure 4b.

Figure 4. Raw (figure 4a) and debanded (figure 4b) TM band 3 image of Padre Bay on Lake Powell. The debanding procedure effectively removes image banding without altering the mean image grey value.

Extracting Image Data

Image grey values were extracted at the image coordinates calculated by the transformation equation. The ARC UNGENERATE command generated an ascii file of sampling site image coordinates from the transformed Arc coverage. Image grey values were extracted at the image coordinates contained in this file, and stored in an ascii file. This file of image grey values was merged with the water quality data file to form the data set on which analysis was performed.

DATA ANALYSIS: DEVELOPING WATER QUALITY PREDICTION MODELS AND PRODUCING WATER QUALITY MAPS

The water quality/TM data set was studied to determine which samples should be excluded from model development, and how to stratify the lake into regions which exhibited consistent relationships between image grey values and chlorophyll-a and Secchi depth values. Multiple regression analysis was then employed to generate chlorophyll-a and Secchi depth prediction models for each of the lake strata. A modified lookup table approach was used to define a single surface temperature prediction model for the entire lake. The models were applied to the TM imagery, producing maps of chlorophyll-a concentration, Secchi depth, and surface temperature. These maps were finalized by color coding, and placing them on a black-and-white image background for geographic reference.

Editing and Stratifying the Water Quality/TM Data Set

The water quality/TM data set was used to define the models which predict water quality parameters from the TM image. Plots of chlorophyll-a concentration and Secchi depth versus the six reflective TM bands were crucial in the development of these models. They helped the analyst determine if certain samples should be excluded from model development, and how the image could be stratified into similar regions to increase model prediction accuracy. When interpreting these plots, the analyst considered the factors that affect water reflectance, the reliability of the sample values, and the limitations of the TM spectral bands for water quality mapping.

Factors Considered When Editing and Stratifying the Water Quality/TM Data Set

Factors Affecting Water Reflectance

The reflectance signal of a lake or reservoir is affected by numerous factors, including those which influence the water's volume reflectance, and those which influence reflectance from the air/water interface. These factors include:

- algal species composition
  Different species of algae have different relationships between spectral reflectance and chlorophyll-a concentration due to:
  - differences in the relative amounts of other pigments like phycocyanin, chlorophyll-b, and chlorophyll-c
  - differences in the absolute amount of chlorophyll-a per cell
  - differences in the size of the cells (Stumpf and Tyler, 1988)
- location of algae in the water column
  The spectral reflectance curve of a given concentration of a given species of algae will change as the algae is moved from shallow to deeper depth (Quibell, 1992). The vertical profile of algae concentration can vary across a lake. For example, variable winds

might result in surface mats of bluegreen algae in calm areas, and cause the mixing of the bluegreens in the water column in windy, wavy areas.

- concentration of DOC (dissolved organic carbon)
  DOC has a reflectance curve in the visible and near IR that is very similar to that of chlorophyll-a. Its presence in a lake, especially if it is not distributed homogeneously, can confound chlorophyll-a mapping efforts (Stumpf and Tyler, 1988; Dierberg, 1992).
- mineral sediment concentration
  Higher concentrations of mineral sediments increase the volume reflectance of water, and interfere with the prediction of chlorophyll concentration (Ritchie et al., 1990; Lathrop et al., 1991).
- sediment color
  The wavelength band best for mapping turbidity cause by green algae may not be the best for mapping turbidity caused by suspended red clays.
- sediment particle size
  Larger suspended sediments produce higher reflectance than smaller suspended particles at the same concentration (Wen-yao and Klemas, 1988).
- zooplankton concentration
  Increasing zooplankton concentration increases the volume reflectance of water.
- zooplankton distribution within the water column
  As with algae, the spectral reflectance of a given concentration of zooplankton will change as the zooplankton move from shallow to deeper depths. Zooplankton will move up and down in the water column to escape predation by fish.
- presence/concentration of flotsam
  Flotsam alters reflectance while not affecting water quality per se.
- sun glint
  Lower solar zenith angles and increased water surface roughness both increase the probability of sun glint.

Information about all of these factors was not available for Lake Powell on 10/14/92. However, some basic knowledge of the lake allowed the analyst to make educated guesses about some of those factors. This knowledge included 1) the flow regimes of tributaries, 2) typical sediment types and concentrations from tributaries, 3) relative temperatures of tributaries and lake water, 4) location of likely nutrient sources that might spur algal growth, 5) sun angle, and 6) wave height.

Factors Affecting Sample Values

The measurements of chlorophyll-a concentration, Secchi depth, and surface temperature were made at single points in space and time on a spatially and temporally variable system. The many successful applications of remotely sensed data to water quality analysis indicate that such point samples can indeed be related to image data. Nevertheless, when developing the water quality prediction models, the analyst considered the following factors:

- accuracy and precision of the reported sample values
  - differences in sample measurement techniques between and within sampling teams
  - differences in sample processing techniques between and within sampling teams
  - degree of subjectivity in the field measurements
  - environmental conditions that could affect field measurements
- scale differences between area of water sampled in the field and the

projected area of a TM pixel
- temporal variability of the sampled parameter and the time between sampling and the satellite overpass
- spatial variability of the sampled parameter and reliability of the sampling positions
    - accuracy of position measurements
    - boat drift

Factors Affecting the Utility of the TM Sensor

Image brightness variations within water bodies typically occupy only a small fraction of the total dynamic range available to the TM sensor. This relatively coarse radiometric resolution limits the capacity of TM data to detect small concentrations of material suspended within the water column.

Another limitation of TM imagery is its spectral resolution. Although the broad-band radiance measurements of TM imagery are quite adequate for mapping water quality parameters such as turbidity and secchi depth that are directly related to water brightness, TM bands are not optimally designed for distinguishing chlorophyll-a concentration. Chlorophyll-a reflectance and absorption in the visible and near IR is highly selective, and within the broad range of TM spectral bands, spectral absorption and reflectance features tend to counteract, resulting in a flattening of the reflectance spectrum (Dekker et al., 1992). The broad range of the TM spectral bands also hinder separating chlorophyll-a reflectance from that of other constituents in the water column (Khorram, 1985).

Editing the Water Quality/TM Data Set

As a result of careful review of the above factors for each sample point, not all of the data collected on 10/14/92 was used to define water quality prediction models. Samples were excluded from consideration during the development of the chlorophyll-a prediction model if:
- they were collected in a heterogeneous region of the lake where a slight positional error could cause a significant change in image grey value
- they were collected in extremely turbid areas within the Colorado or San Juan Rivers
  The extremely high reflectance from the rivers was exclusively due to a high concentration of suspended mineral sediment, whereas the lake reflectance came primarily from a mixture of algae and mineral sediment. Grey values from the rivers and the lake were significantly different, and could not be used together during regression model development.
- their chlorophyll-a values were less than 1 μg/l
  The TM data could not reliably estimate chlorophyll-a concentrations of less than 1 μg/l. Including those samples in the data set introduced a large amount of variability. The regression model was then forced to minimize error in the noisy, and more numerous low chlorophyll-a values at the expense of the better behaved, but less numerous higher chlorophyll-a values. Even though the samples with chlorophyll-a values of less than 1 μg/l were excluded from regression model development, the maximum prediction error for any of the excluded points was only 1 μg/l.

Secchi depth measurements were excluded from consideration during model development if they were made:
- in a heterogeneous region of the lake where a slight positional error could cause a significant change in image grey value
- at extremely turbid areas within the Colorado or San Juan Rivers. These rivers were much more turbid than the lake

Secchi measurements taken in the rivers did not follow the trend established by the lake measurements.

- more that 3.5 hours before or after solar noon
  This limitation reduced Secchi depth measurement variation due to sun angle differences while still leaving a large data set for regression analysis. (Data supporting the correlation between Secchi depth and solar zenith angle is given in Appendix A).

Stratifying the Lake

Study of the data also revealed that developing separate prediction models for three different regions of the lake improved model results. These strata were: 1) the Colorado River inflow area, 2) the San Juan River inflow area, and 3) the main body of the lake (figure 5). Relationships between chlorophyll-a and Secchi depth values and image grey values were generally good within strata, but not across strata. The need for this stratification probably relates to differences in suspended sediment concentration and composition from the Colorado and San Juan Rivers, and the comparative lack of suspended mineral sediments in the other parts of the lake.

Mapping Chlorophyll-a Concentration and Secchi Depth

Regression Analysis Guidelines

Multiple regression analyses were performed on the edited and stratified water quality/TM data sets to generate models which predict chlorophyll-a concentration and Secchi depth from de-banded and averaged image data. Within each stratum, all possible regressions were performed with the six reflective TM bands as independent variables and the chlorophyll-a and Secchi values (including square roots and natural logs) as the dependent variables. The square root and natural log transformations were applied to the chlorophyll-a and Secchi data because they sometimes help to linearize the relationship between the TM and the water quality data. A listing of model independent variables and their associated r^2 values showed which regression models were worthy of further investigation. From this list, the most promising regression models were calculated with more complete regression output.

R-squared values alone were not used to determine the final model selected. Increasing the number of independent variables in almost any regression model will increase the r^2 value. However, the more independent variables one adds to a given model, the greater the chances that the model is data set dependent and does not represent the true relationship within the population. For this reason, only those independent variables which were significant at the 0.95 probability level were included in the regression models.

Mapping Chlorophyll-a Concentration

Chlorophyll-a content, as in indicator of algal standing stock, is an important indicator of lake biological productivity and water quality. Two chlorophyll-a measurements were available for each sample site: the surface and 0-5 meter composite. These two different measurements were highly correlated ($r^2 = 0.9706$), with a maximum difference of 1.90 μg/l. Separate regression analyses were performed using each of these two measurements as the dependent variable. Because the 0-5 meter composite chlorophyll-a values produced slightly higher r^2 values than the surface chlorophyll-a values, the 0-5 meter composite values were mapped.

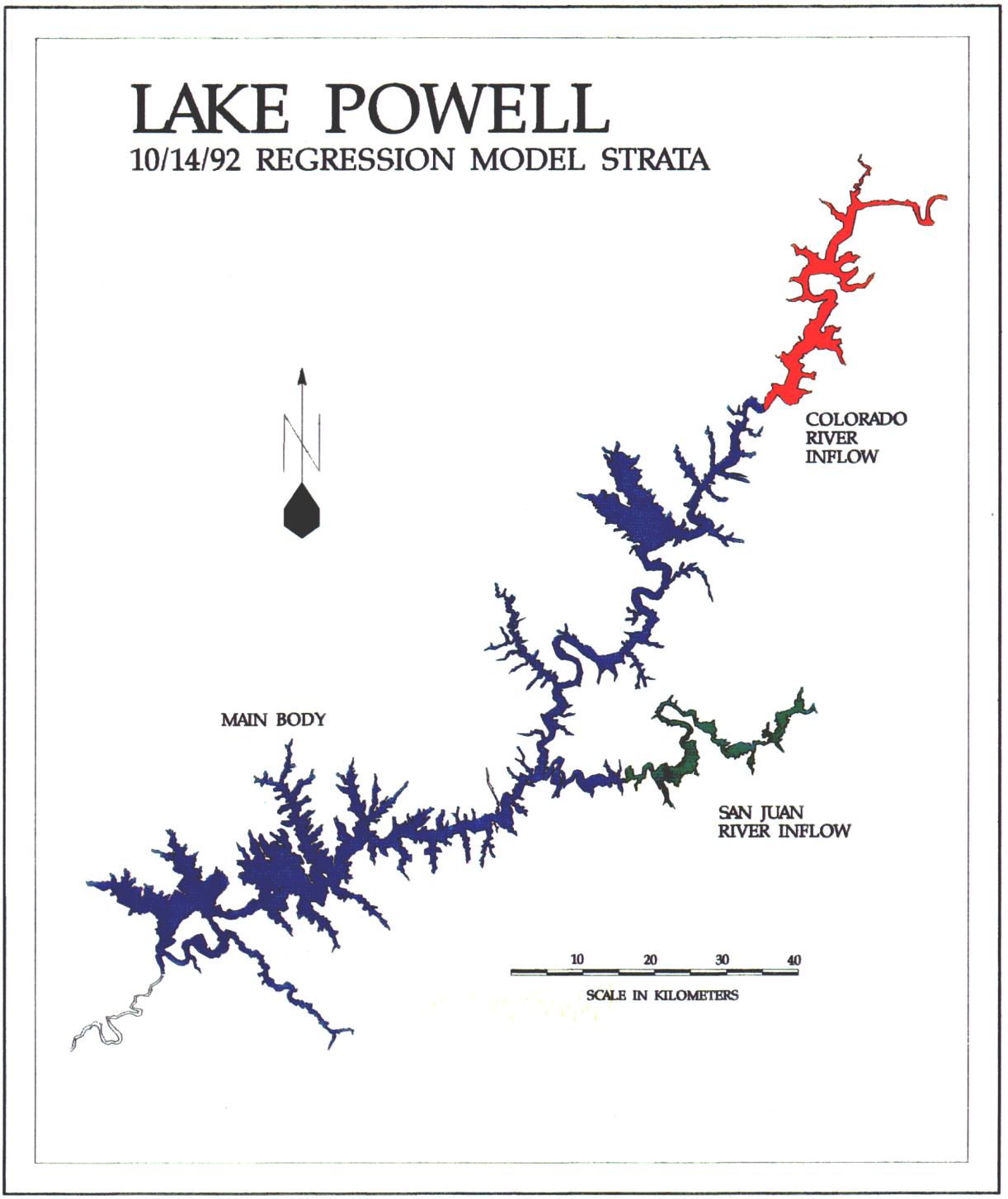

Figure 5. Regression model strata developed for the 10/14/92 Lake Powell TM scene.

The 10/14/92 Lake Powell Chlorophyll-a Concentration Map

Stratifying the lake into three separate regions dramatically improved regression model results. The best chlorophyll-a regression model derived from the non-stratified data had ln chlorophyll-a as its dependent variable. Even when all six reflective TM bands were used as predictors, an r^2 value of only 0.6144 was achieved. Regression models developed from the Colorado River inflow, San Juan River inflow, and main body strata were vast improvements with r^2 values of 0.9008, 0.9401, and 0.9241, respectively (figures 6, 7, and 8). These models were accurate within lake strata, but not across strata.

Each regression model was applied to all pixels falling within its stratum. No anomalous patterns were observed for the San Juan or main body strata, but the Colorado River inflow regression model predicted anomalously high chlorophyll values for those pixels falling within the Colorado River plume. The plume is a transition zone between the free-flowing Colorado River in Cataract Canyon and the calm waters of Lake Powell. The plume has a current which keeps extremely high sediment concentrations in suspension. The high reflectance from these suspended sediments caused the overestimation by the chlorophyll regression model. On 10/14/92, the plume extended only a short distance to near the confluence of the Dirty Devil River before it plunged below the surface waters of Lake Powell.

The overestimation problem was solved by simply masking out the relatively small area of the Colorado River plume, and assigning the chlorophyll values within this area an arbitrary value of 1 μg/l. Waters with extremely high suspended sediment concentrations always have low chlorophyll concentrations because the sediments reflect and absorb incoming sunlight before it can be used for photosynthesis by algae (Verdin and Wegner, 1983).

The modified Colorado River inflow chlorophyll-a concentration map was mosaicked with the San Juan and main body maps to form the final 0-5 m

---

Dependent Variable: CHLA

Analysis of Variance

Source	DF	Sum of Squares	Mean Square	F Value	Prob>F
Model	2	30.75394	15.37697	48.758	0.0001
Error	17	5.36134	0.31537		
C Total	19	36.11528			

Root MSE	0.56158	R-square	0.8515
Dep Mean	3.67300	Adj R-sq	0.8341
C.V.	15.28946		

Parameter Estimates

Variable	DF	Parameter Estimate	Standard Error	T for H0: Parameter=0	Prob > |T|
INTERCEP	1	-11.898862	1.58261526	-7.518	0.0001
TM35	1	1.250175	0.13873418	9.011	0.0001
TM75	1	-1.677687	0.37238628	-4.505	0.0003

Figure 6. Chlorophyll-a regression model for the Colorado River inflow stratum.

Dependent Variable: CHLA

Analysis of Variance

Source	DF	Sum of Squares	Mean Square	F Value	Prob>F
Model	2	116.08117	58.04059	40.689	0.0001
Error	12	17.11722	1.42644		
C Total	14	133.19839			

Root MSE	1.19433	R-square	0.8715
Dep Mean	4.32348	Adj R-sq	0.8501
C.V.	27.62438		

Parameter Estimates

Variable	DF	Parameter Estimate	Standard Error	T for H0: Parameter=0	Prob > |T|
INTERCEP	1	-18.900104	3.84859189	-4.911	0.0004
TM25	1	2.251583	0.25719765	8.754	0.0001
TM45	1	-1.640225	0.49346017	-3.324	0.0061

Figure 7. Chlorophyll-a regression model for the San Juan River inflow stratum.

Dependent Variable: CHLA

Analysis of Variance

Source	DF	Sum of Squares	Mean Square	F Value	Prob>F
Model	3	37.32559	12.44186	64.308	0.0001
Error	30	5.80418	0.19347		
C Total	33	43.12977			

Root MSE	0.43986	R-square	0.8654
Dep Mean	1.73443	Adj R-sq	0.8520
C.V.	25.36018		

Parameter Estimates

Variable	DF	Parameter Estimate	Standard Error	T for H0: Parameter=0	Prob > |T|
INTERCEP	1	8.741902	1.46101575	5.983	0.0001
TM15	1	-0.483464	0.06035993	-8.010	0.0001
TM25	1	0.850491	0.09323798	9.122	0.0001
TM75	1	0.350582	0.08823783	3.973	0.0004

Figure 8. Chlorophyll-a regression model for the main body stratum.

chlorophyll-a concentration image map (figure 9). The image map shows that the vast majority of Lake Powell is oligotrophic with chlorophyll-a concentrations hovering around 1 μg/l. A few areas of elevated chlorophyll-a concentration are located near the Colorado, San Juan, and Escalante River

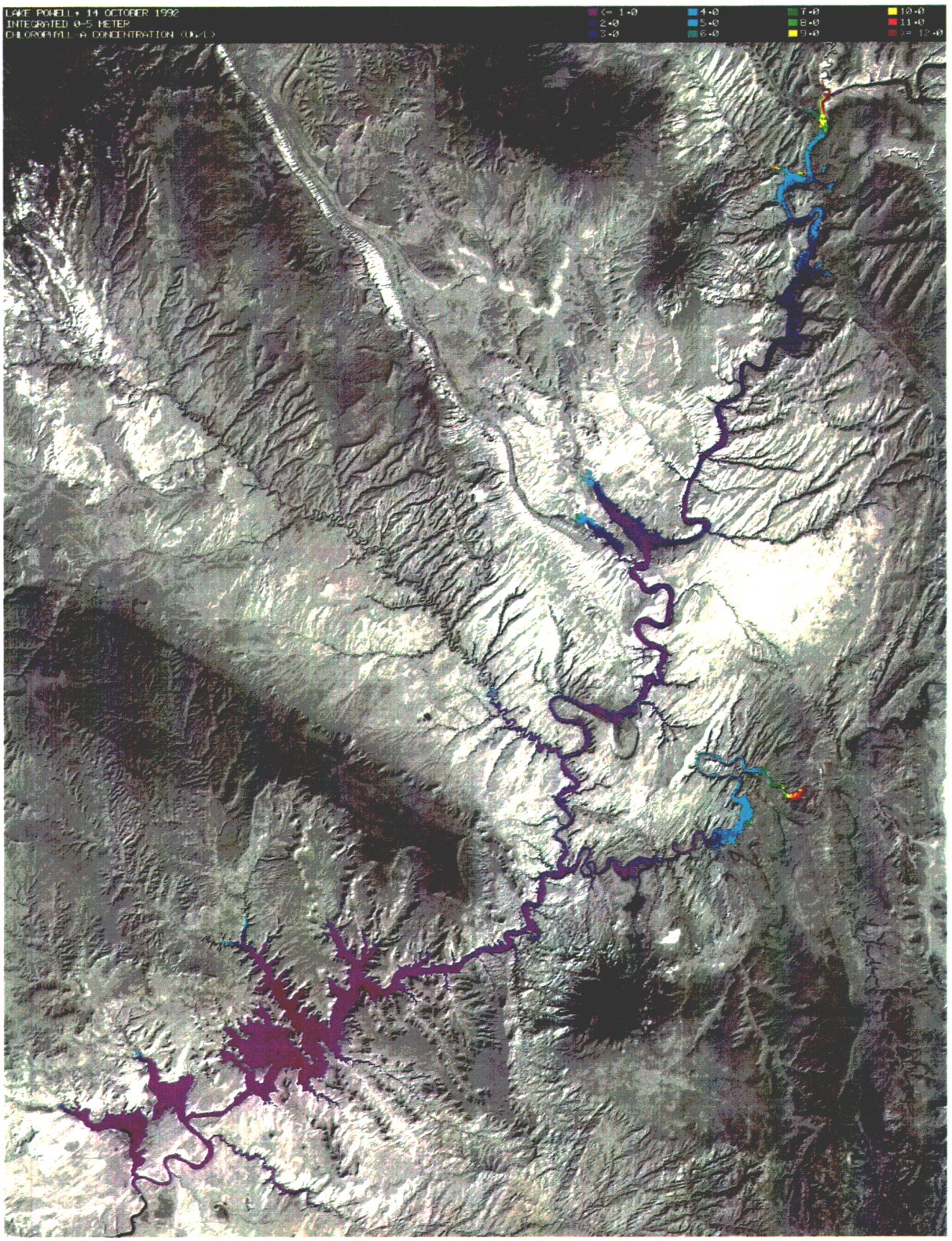

Figure 9. Chlorophyll-a concentration image map for Lake Powell on 10/14/92.

inflow areas, as well as the upper ends of some of the bays. Even in these areas, the chlorophyll levels are still quite low (maximum of 12 μg/l).

Mapping Secchi Depth

Secchi depth is a common measurement of overall water clarity. It is made by lowering a white disc 20 cm in diameter into the water on a calibrated line. The depth at which the disc disappears is known as the Secchi disc transparency, or Secchi depth.

Secchi depth measurements depend on several factors, including 1) the eyesight of the viewer, 2) the contrast between the disc and the surrounding water, 3) the reflectance of the disc, 4) the diameter of the disc (in extremely clear waters only), 5) wave and sun angle conditions which determine the amount of sun glint with which the viewer must contend, and 6) illumination intensity (as determined by sun angle and cloud cover).

Ideally, Secchi depth should be measured from the shady side of the boat to minimize sun glint in the eyes of the person taking the measurement. It should also be measured between 10:00 am and 2:00 pm to minimize variation in illumination intensity (Cole, 1979). However, illumination intensity also varies with time of year. This variation can affect Secchi depth measurements, especially in clear water (see Appendix A).

Secchi depth is well suited for mapping using TM imagery because the suspended and dissolved organic and inorganic materials that affect Secchi depth also affect reflectance in the TM visible and near-IR bands. The relationships between TM grey values and Secchi depth can vary however, depending on spectral reflectance of the constituents within the water column.

The 10/14/92 Lake Powell Secchi Depth Map

As with the chlorophyll-a data, stratification improved regression model results, although not as significantly as with the chlorophyll-a data. The best Secchi regression model derived from the non-stratified data had ln Secchi depth as its independent variable. When all six reflective TM bands were used as predictors, an r^2 value of 0.8855 was achieved. Regression models developed from the Colorado River inflow, San Juan River inflow, and main body strata used only one or two TM bands as predictors and improved the r^2 values to 0.9008, 0.9401, and 0.9241, respectively (figures 10, 11, and 12). As with chlorophyll-a regression models, these models were accurate within lake strata, but not across strata.

Each regression model was applied to all pixels falling within its stratum. The strata were then mosaicked together to generate the predicted Secchi depth image map (figure 13). This map shows high turbidity at the inflow of the Colorado, San Juan, and Escalante Rivers, as well as elevated turbidity in most of the larger embayments. The main channel of Lake Powell south of Bullfrog Basin is relatively clear (Secchi depths of 9 meters or more), with clearest water occurring in and around Padre Bay.

Transforming Image Data

Predictor variables other than debanded and averaged TM grey values have been used to predict chlorophyll-a and Secchi depth using TM data. Two of the more common transforms, principal components and band ratios, were investigated for use with the 10/14/92 Lake Powell image. Neither of these transforms were used to predict water quality parameters for the 10/14/92 Lake Powell TM scene, but they are discussed in Appendix B because of their possible utility

Dependent Variable: LNSECCHI

Analysis of Variance

Source	DF	Sum of Squares	Mean Square	F Value	Prob>F
Model	2	4.24692	2.12346	90.838	0.0001
Error	20	0.46753	0.02338		
C Total	22	4.71445			

Root MSE	0.15289	R-square	0.9008
Dep Mean	1.01364	Adj R-sq	0.8909
C.V.	15.08354		

Parameter Estimates

Variable	DF	Parameter Estimate	Standard Error	T for H0: Parameter=0	Prob > |T|
INTERCEP	1	3.315543	0.65619426	5.053	0.0001
TM25	1	-0.222717	0.01760154	-12.653	0.0001
TM45	1	0.217374	0.08862348	2.453	0.0235

Figure 10. Secchi depth regression model for the Colorado River inflow stratum.

Dependent Variable: LNSECCHI

Analysis of Variance

Source	DF	Sum of Squares	Mean Square	F Value	Prob>F
Model	1	22.71038	22.71038	572.628	0.0001
Error	47	1.86402	0.03966		
C Total	48	24.57440			

Root MSE	0.19915	R-square	0.9241
Dep Mean	1.98473	Adj R-sq	0.9225
C.V.	10.03400		

Parameter Estimates

Variable	DF	Parameter Estimate	Standard Error	T for H0: Parameter=0	Prob > |T|
INTERCEP	1	5.932595	0.16741296	35.437	0.0001
TM25	1	-0.231493	0.00967388	-23.930	0.0001

Figure 11. Secchi depth regression model for the San Juan River inflow stratum.

Dependent Variable: LNSECCHI

Analysis of Variance

Source	DF	Sum of Squares	Mean Square	F Value	Prob>F
Model	2	7.79050	3.89525	102.084	0.0001
Error	13	0.49604	0.03816		
C Total	15	8.28654			

Root MSE	0.19534	R-square	0.9401
Dep Mean	1.73977	Adj R-sq	0.9309
C.V.	11.22783		

Parameter Estimates

Variable	DF	Parameter Estimate	Standard Error	T for H0: Parameter=0	Prob > |T|
INTERCEP	1	8.254384	0.78618216	10.499	0.0001
TM25	1	-0.516353	0.03614731	-14.285	0.0001
TM45	1	0.226471	0.07634020	2.967	0.0109

Figure 12. Secchi depth regression model for the main body stratum.

in future studies.

Mapping Surface Temperature

TM6, the thermal channel, was used to map surface temperature. TM6 measures thermal radiation emitted from objects on the earth's surface. The amount of emitted thermal radiation is directly related to surface temperature. A LUT (lookup table) relates TM6 image grey values to radiant temperatures (Bartolucci and Chang, 1988). The radiant temperatures in the LUT are the temperatures a perfect black body must be in order to emit the amount of thermal radiation corresponding to each TM6 grey value. However, radiant temperatures measured at satellite altitudes rarely equal earth surface temperatures due to influences of the atmosphere and the surface itself.

Factors which alter the amount of thermal radiation the TM sensor records from any given target are both additive and multiplicative in nature. Reduction of the thermal radiation emitted from a warm lake by a thin layer of cold cirrus clouds is an example of additive alteration. Multiplicative effects are caused by anything that affects the emitted thermal radiation proportionally to its intensity. For example, the emissivity of an object and the attenuation of thermal radiation by water vapor or other gasses in the atmosphere, are both multiplicative effects. It is necessary to correct for effects of thermal emissivity and the atmosphere before accurate surface temperature maps can be generated.

Modified Lookup Table Correction

A modified LUT approach was used to predict surface temperatures from TM6 grey values. This method involves the simple rescaling of LUT temperatures by a

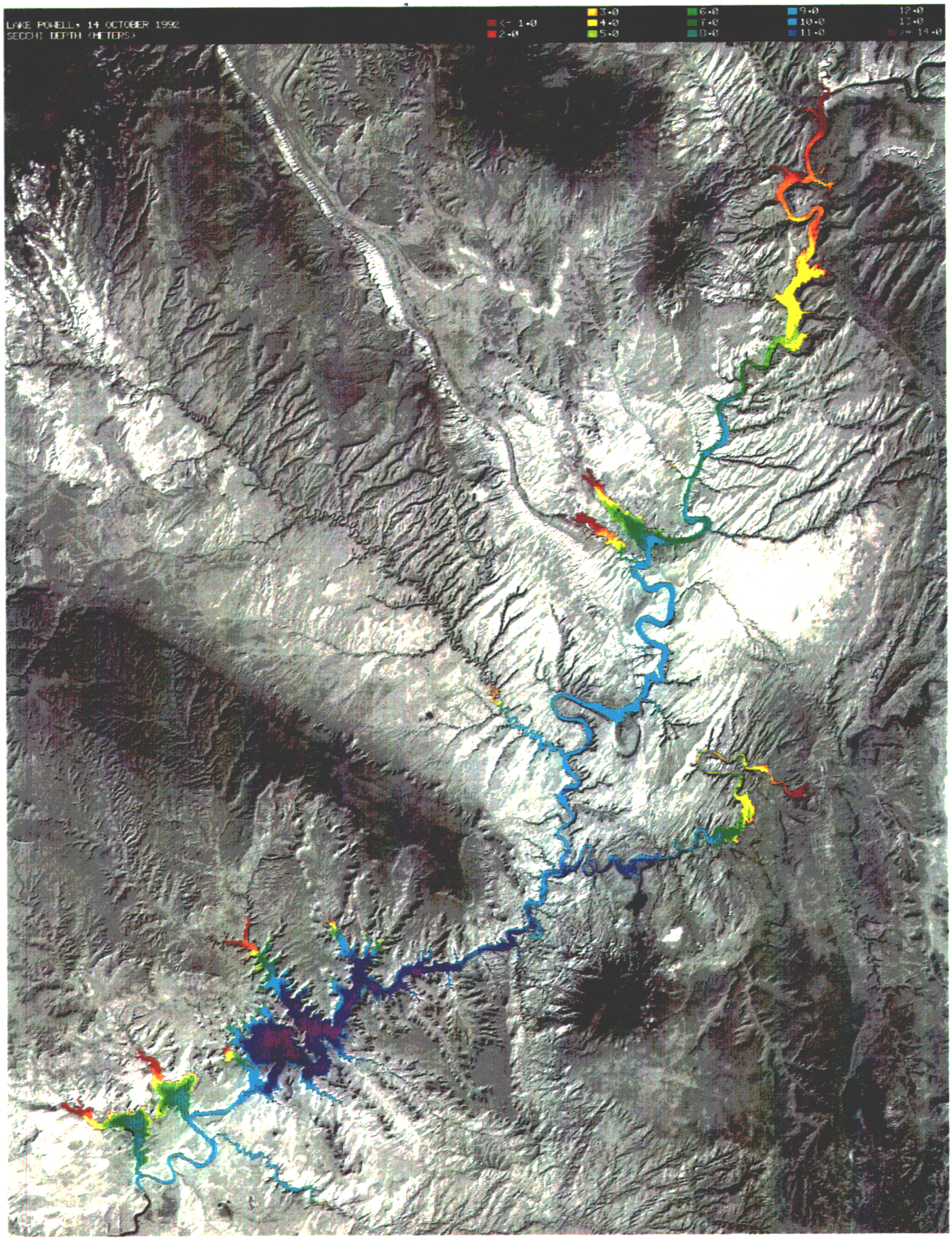

Figure 13. Secchi depth image map for Lake Powell on 10/14/92.

constant correction factor. The correction factor was calculated by subtracting the average of all surface temperature measurements made within one-half hour of the satellite overpass, from the LUT temperature corresponding to the average TM6 grey value for the same sampling sites. This one-hour window was selected to limit the degree of warming or cooling of surface water that could occur between the time of sampling and the satellite overpass. A map of predicted surface temperatures was created by simply rescaling the TM6 image by the amount of the correction factor.

This procedure corrects for additive and multiplicative factors for a single point in the lookup table. However, it does not correct for multiplicative factors which change the slope of the TM6/surface temperature relationship relative to the TM6/radiant temperature relationship (figure 14). Figure 14a shows a hypothetical relationship between TM6 grey values and both radiant temperatures (dashed line) and surface temperatures (solid line). Figure 14b shows the effect of the LUT correction. Temperature values from the corrected TM6 lookup table equal surface temperature at the point of correction, but diverge at higher and lower temperatures. However, the magnitude of the error (the vertical distance between the two lines) is usually slight because 1) the high emissivity of water and typically low atmospheric absorption of thermal radiation limits the slope differences between the two lines, and 2) the small temperature ranges typically found within water bodies limits the distance on the graph over which temperature differences can accumulate. Several investigators have compared LUT temperatures with measured water temperatures, and shown RMS errors smaller than 1 degree Celsius (Anuta et al., 1984; Malaret et al., 1985; Lathrop and Lillesand, 1987).

Regression Modelling

An alternative method to the modified LUT procedure is a regression model similar to those developed for chlorophyll-a and Secchi depth which predicts surface temperature from TM6 grey values. This technique is useful only when several teams sample a lake, so that the number of samples collected within 30 minutes of the satellite overpass is large enough to produce a reliable regression. Furthermore, the full range of surface water temperatures on the lake should be sampled to adequately define the regression model. Although this procedure will produce maps showing the same patterns as the modified LUT technique, its absolute temperature measurements are less reliable due to its increased susceptibility to measurement error. The modified LUT procedure uses the average of several temperature and TM6 grey value measurements to determine only one parameter: the additive correction factor. It uses the sensor gain factor calculated in the laboratory prior to launch, instead of calculating a gain factor from the data. The regression technique typically uses a small data set to determine both the sensor gain and offset. The small data set size enhances the importance of extreme values, so individual measurement errors can have a more dramatic effect.

Potential Error Sources

Both the modified LUT and regression techniques can be adversely affected by non-homogeneous atmospheric conditions. Variations in atmospheric attenuation across the image will produce artificial temperature variations in the output temperature map. There was some variation in atmospheric condition in the 10/14/92 Lake Powell scene. Conditions ranged from completely clear to high, thin scattered clouds; but the clouds were not thick enough to cause noticeable variation in the output map.

Another factor that can affect both the modified LUT and regression techniques is sun glint. The TM6 band measures radiation in the thermal region of the electromagnetic spectrum (10.4 - 12.5 μm). For nearly all earth surfaces, the

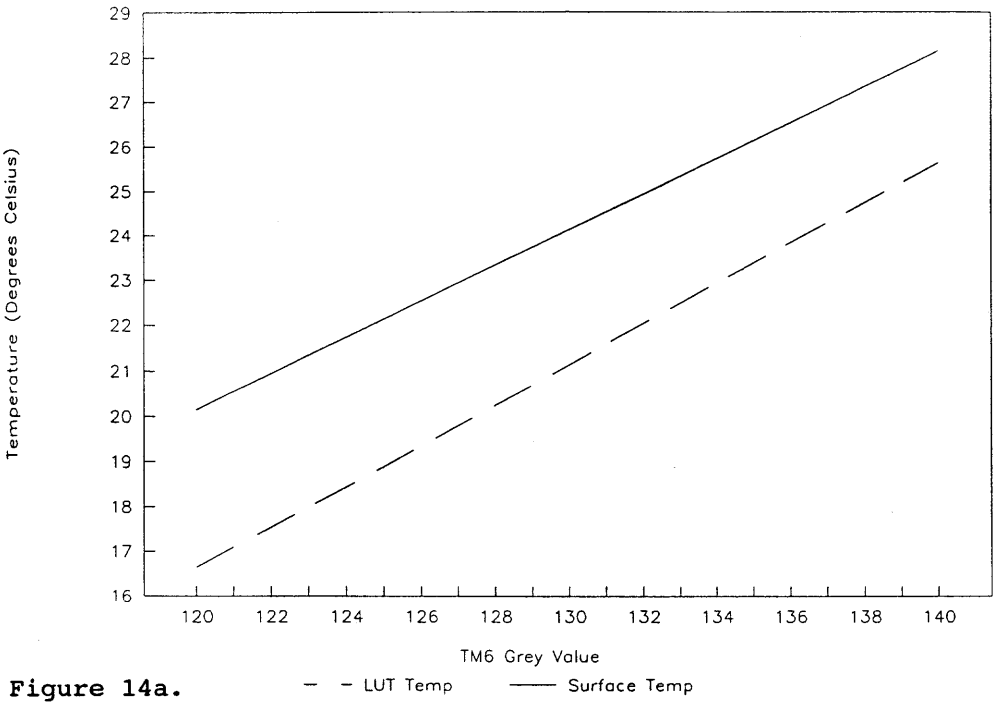

Figure 14a.

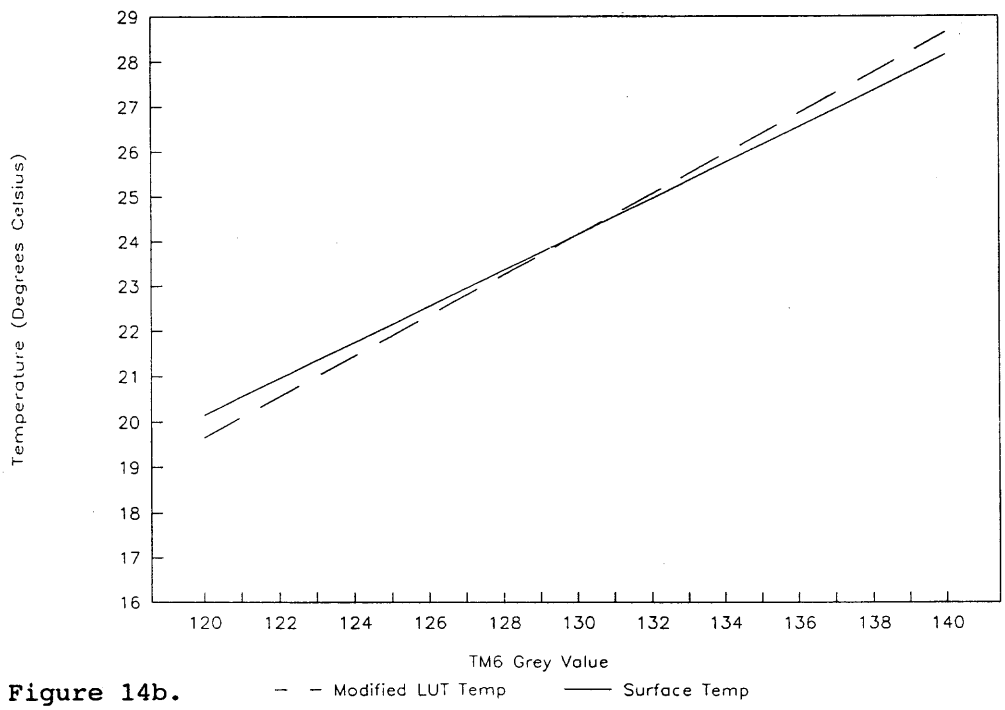

Figure 14b.

Figure 14. Graphic representation of the modified LUT correction. Figure 14a shows a hypothetical relationship between TM6 grey values and both LUT temperatures (dashed line) and surface temperatures (solid line). Figure 14b shows the effect of the LUT correction. LUT temperatures are close to actual temperature near the calibration temperature, and never diverge far from actual temperatures over the limited temperature range found on most lakes and reservoirs.

vast majority of the radiation in this wavelength band is emitted, not reflected. However, TM6 is not completely insensitive to reflected radiation. Therefore, areas of sun glint which contain high amounts of reflected solar radiation can elevate TM6 grey values. It is possible to get elevated temperature readings on the order of 2 degrees Celsius in areas of sun glint (Brush, 1993). Areas of sun glint can be identified by visually inspecting TM7 for anomalous patterns on the lake surface. TM7 has practically no water penetration, and is generally not sensitive to constituents within the water column. For this reason, noticeable patterns on the lake surface seen on a TM7 image probably indicate areas of sun glint. Band 7 of the 10/14/92 Lake Powell scene contained no noticeable patterns. Sun glint-induced elevated temperature estimates therefore were not considered to be a problem.

The 10/14/92 Lake Powell Surface Temperature Map

Figure 15 shows the surface temperature image map of Lake Powell for 10/14/92. Aside from the northernmost part of the lake where cooler water from the Colorado River is at the surface, the lake shows only about one degree of temperature variation. The narrow canyons in the central portion of the lake show the warmest temperatures. One explanation is that wind speed may be reduced in the protected narrow canyons compared to the more open bays. Decreased wind velocity reduces evaporative cooling, and reduces wave action that mixes warmer surface water with cooler water below. Another explanation is that narrow canyons act as radiation traps and allow less radiative cooling to the sky than flat terrain.

Generating Hardcopy Maps

Final water quality maps were color-coded for ease of interpretation. Separate RGB (red, green, and blue) component images were generated from each map which, when combined, produced the desired color coding. The piecewise linear remapping functions used to generate the three component images are shown as the red, green, and blue lines in figure 16. The lowest chlorophyll-a concentration and surface temperature values, and the highest Secchi depth value were assigned an X-axis value of zero (corresponding to the color violet). The highest chlorophyll-a concentration and surface temperature values, and the lowest Secchi depth value were assigned an X-axis value of 255 (corresponding to the color red). Intermediate values were linearly interpolated between 0 and 255. End points and inflection points of the colored lines in figure 16 define the breakpoints for each of the three piecewise linear mapping functions. X-values of these breakpoints were converted back to their particular chlorophyll, temperature, or Secchi depth values, and the Y-values were taken directly from the Y axis. For example, if the chlorophyll-a image had a data range of 0 to 25.5 μg/l, the remapping function for the red component would be:

```
from = (  0.0  3.2  14.4   20.0   25.5)
to   = (144    0     0    255    255  ).
```

Final image maps were generated by placing the color coded maps onto a black-and-white image background for geographic reference, and adding a color-coded legend at the top.

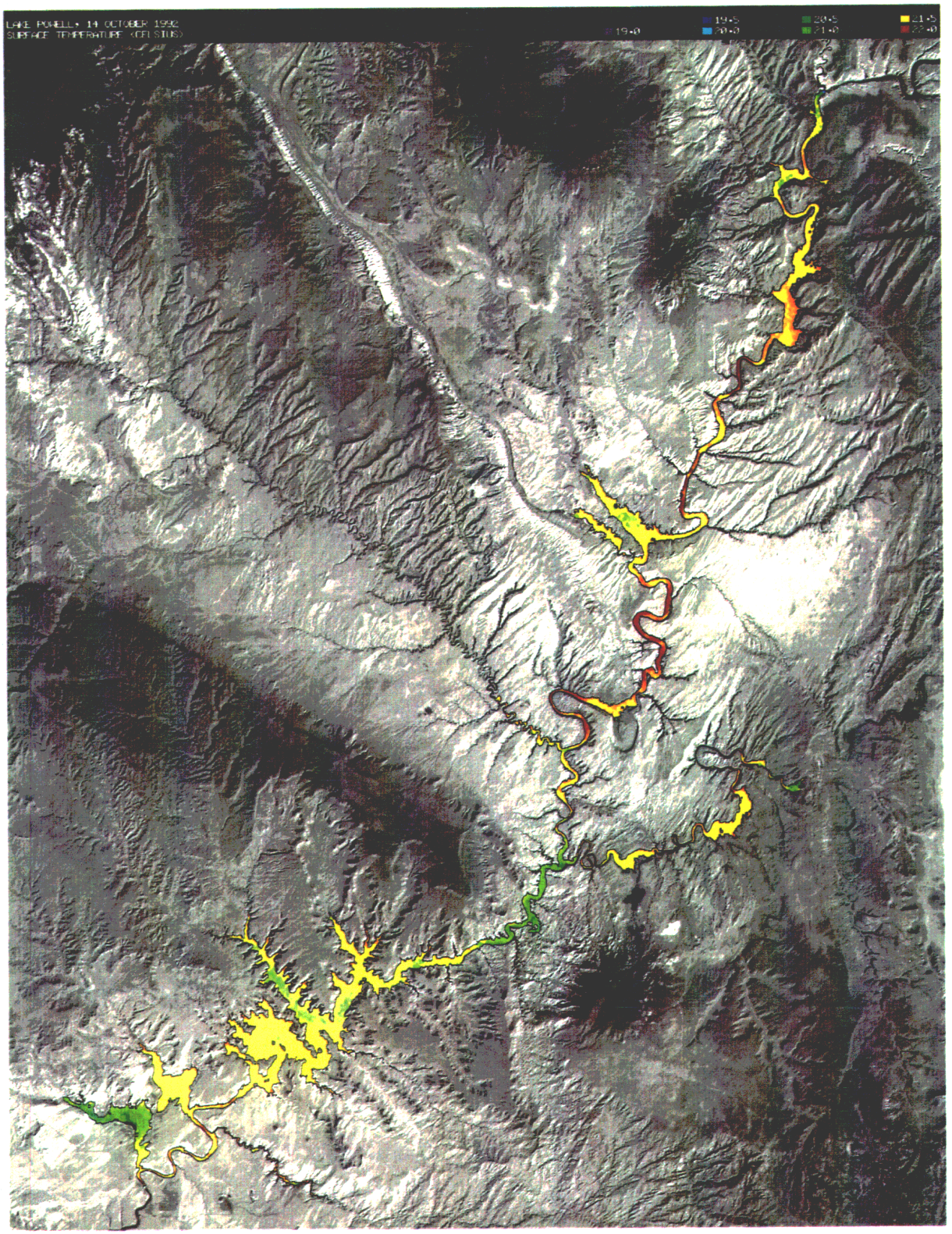

Figure 15. Surface temperature image map for Lake Powell on 10/14/92

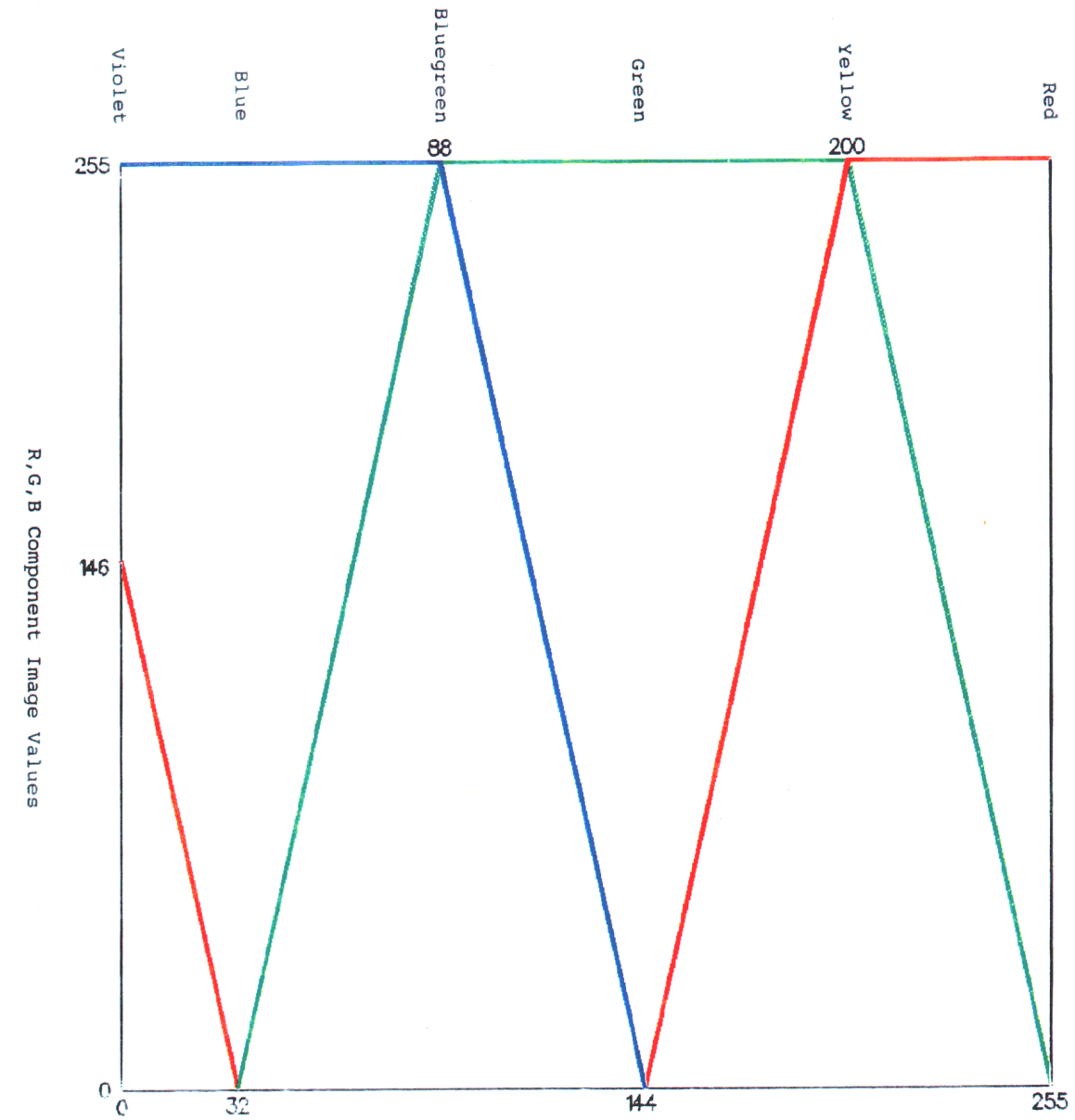

Figure 16. Remapping functions used to convert images of predicted temperature, chlorophyll-a concentration, and Secchi depth values to color coded image maps.

SUMMARY AND CONCLUSIONS

10/14/92 Lake Powell Water Quality Maps

A Landsat TM image of Lake Powell acquired on 10/14/92 was successfully used to map chlorophyll-a concentration, Secchi depth, and surface temperature. The TM imagery was first preprocessed to reduce image banding and random noise. A coordinate transformation equation was then developed which related UTM coordinates with image row/column coordinates. This coordinate transformation was applied to GPS-derived positions of sampling boats to determine their locations on the image. Image grey values were then extracted from the image at the calculated row/column coordinates, and merged with a corresponding file of water quality parameters to form the water quality/TM data set.

After careful removal of selected samples from the water quality/TM data set, multiple linear regression analyses were used to develop models which predict chlorophyll-a concentration and Secchi depth from preprocessed TM image grey values. The limnological complexity of Lake Powell forced its stratification into three distinct regions, each with its own chlorophyll-a and Secchi depth prediction model. The regression models were applied to their respective strata, and the strata were mosaicked together to form the final water quality maps.

To generate the surface temperature map, lake temperatures measured within one half hour of the Landsat overpass were used to quantify the offset between surface temperatures and TM6 lookup table temperatures. Once this offset was known, generating a surface temperature image map was a simple matter of rescaling the TM6 image.

The water quality maps were color coded and placed in a black-and-white image background to form the final image maps. These image maps provide a unique view of three water quality parameters for a single point in time. The imagery fills in the gaps between point sampling stations, and shows spatial patterns that are undetectable using point sample data alone. The image maps are useful to limnologists studying lake productivity, circulation, and evaporation, and can be used as a tool to more intelligently distribute lake sampling teams during future lake surveys.

Future Research Directions

Although TM images can produce useful maps of water quality, there is room for improvement in the areas of spectral and radiometric resolution. Optimal placement of spectral bands will offer the opportunity to discern the reflectance and fluorescence signal of chlorophyll-a in the midst of other water constituents (Dierberg, 1992). More sensitive detectors will produce a larger dynamic range over water targets, thereby increasing the precision of water quality parameter estimates.

Improved data from spaceborne sensors will most likely have to wait until the launch of MODIS (Moderate Resolution Imaging Spectrometer) around 1998. Its 250-meter spatial resolution will limit its use to larger water bodies, but its multitude of spectral bands will improve its utility for water quality remote sensing.

Improved data are available today from aircraft-mounted imaging spectrometer or adjustable-band sensor systems. Three such sensors include CASI (Compact Airborne Spectrographic Imager), AMMS (Airborne Multispectral Measurement System), and AVIRIS (Advanced Visible and Infrared Imaging Spectrometer). CASI can produce 288 bands of data in profile mode, or up to 12 user-selected bands of imagery over a 512 pixel swath (Dierberg, 1992). AMMS is a

calibrated video system that can produce 512 by 512 images in a maximum of six user-specified spectral bands (Dierberg, 1992). AVIRIS is a true imaging spectrometer that acquires 224 bands of imagery over a 550-pixel wide swath (Lillesand and Kieffer, 1987). Imagery acquired from these sensors is typically more expensive than imagery acquired from spaceborne sensors due to the cost of aircraft operation. Imagery from airborne sensors also require more geometric processing than that from spaceborne sensors due decreased platform stability and larger scan angles. However, high-accuracy GPS receivers are being integrated into airborne sensor systems, making the geometric registration of scenes less problematic.

If funding permits, the flexibility of aircraft scheduling and the desirability of the spectral and radiometric resolution of the sensors described above makes airborne remote sensing of water quality on Lake Powell an attractive option. Although more complicated geometric processing would be required, optimally placed spectral bands could deconvolve the additive effects of the multitude of water column constituents, producing more reliable maps of water quality parameters than are possible from TM data. Such data might remove the need to stratify Lake Powell and provide more accurate maps of water quality.

APPENDIX A
APPARENT DEPENDENCE OF SECCHI DEPTH WITH SOLAR ZENITH ANGLE

Secchi depth variation due to differences in sun angle was demonstrated in the 10/14/92 Lake Powell data set. Differences in duplicate Secchi readings made at different times of day with similar wind and wave conditions showed a marked correlation with the change in sun angle. For eleven duplicate samples, differences in secchi depth were accurately predicted (r^2 of 0.9341) from differences in the cosine of the solar zenith angle and the higher of the two duplicate secchi depth measurements (figure A-1).

$$\Delta S = -1.66482 + 4.63428\ (\Theta z_{max} - \Theta z_{min}) + 0.212738\ (S_{max})$$
$$r^2 = 0.9341$$

where:

S_{max} = higher Secchi depth measurement
S_{min} = lower Secchi depth measurement
$\Delta S = S_{max} - S_{min}$
Θz_{max} = cosine of the solar zenith angle for the higher sun angle
Θz_{min} = cosine of the solar zenith angle for the lower sun angle

Figure A-1. A regression model used to predict differences in duplicate Secchi depth measurements based upon sun angle differences at the time of measurement.

Cosine of the solar zenith angle was used in the model because it is directly related to the direct beam solar radiation intensity. A more accurate predictor variable might have been total incoming solar radiation (direct and diffuse sunlight). This value is more difficult to calculate, and its use was not investigated due to lack of time. Although these results are from a limited data set, they indicate the possibility of being able to normalize secchi depth measurements to a common sun angle, and to remove some of the variation found with secchi depth measurements. This is an area for further research.

APPENDIX B
TRANSFORMED IMAGE DATA

Predictor variables other than debanded and averaged TM grey values have been used to predict chlorophyll-a and Secchi depth using TM data. Two of the more common transforms, principal components and band ratios, were investigated for use with the 10/14/92 Lake Powell image. Neither of these transforms were used in the water quality prediction models for the 10/14/92 Lake Powell TM scene, but they are discussed here because of their possible utility in future studies.

Principal Components

PCs (principal components) have been used with some success for water quality mapping. For a reservoir in Kentucky, Lira et al., 1992, reported r^2 values of 0.63 and 0.95 for turbidity and 0.56 and 0.77 for chlorophyll-a concentration from August and December, 1988 TM scenes, respectively. PCs used for water quality mapping are derived from pixels falling within water bodies. Because PCs are scene dependent, variation in the composition of the sediment, algae, and dissolved substances within the lake, as well as with the amount of atmospheric haze and sun glint will affect the eigenvector coefficients. This variability from image to image precludes simple interpretation rules for all but the first PC.

PC1 contains the majority of the variation in the data set, and its eigenvector entries are typically all positive. Therefore, it depicts general image brightness, and is useful to map water quality parameters which are correlated to broad-band image brightness (e.g. turbidity).

The remaining PCs typically contain a mixture of positive and negative values within their eigenvectors, and therefore measure some aspect of water color. PCs generated from four different dates of TM imagery of Lake Mead show that eigenvector coefficients may change sign and magnitude from one date to another (table B-1). Relationships between any of the PCs and water quality parameters are therefore data set dependent.

Table B-1 shows that for the Lake Mead TM scenes, PC3 through PC6 contain only a small fraction of the total variation in the input image. As this fraction decreases from PC3 to PC6, image noise becomes more and more noticeable, reducing the utility of the higher numbered PCs for water quality mapping. In particular, those PCs with high TM5 and TM7 coefficients have the most noticeable noise problems due to the high noise levels inherent in these two bands.

PCs were not generated for the 10/14/92 Lake Powell image because of the processing time necessary to produce them, and because they were not expected to significantly improve upon the regression results obtained from the raw TM data. This expectation is based upon analysis of a TM image of Lake Mead acquired on 8/23/91. Lake Mead is similar to Lake Powell in many respects. Both are extremely large reservoirs located along the Colorado River, and both are limnologically complex with multiple tributaries which affect the spectral reflectance and biological productivity of their inflow areas. On 8/23/91, samples were collected from all across Lake Mead for correlation with the TM data. PCs were compared to the raw TM bands for their utility for predicting chlorophyll-a concentration and Secchi depth. In both cases, the PCs did not improve upon the r^2 values generated from the raw data.

Failure of PCs to improve upon the results from the raw data for a single image of Lake Mead does not mean that PCs will never have value for water quality mapping on Lake Powell. However, time and budget restrictions precluded any investigations of PCs for the 10/14/92 Lake Powell image.

Date	Eigen Vector Number	TM1 coeff	TM2 coeff	TM3 coeff	TM4 coeff	TM5 coeff	TM7 coeff	Percent of Total Data Variation
8/23/91	1	0.5859	0.5262	0.5850	0.1793	0.0688	0.0258	83.97
9/24/91	1	0.5837	0.5213	0.5926	0.1800	0.0578	0.0256	86.32
7/24/92	1	0.6687	0.5452	0.4601	0.1679	0.1184	0.0421	83.72
8/09/92	1	0.4957	0.5397	0.6258	0.2400	0.1104	0.0409	84.14
8/23/91	2	0.6975	0.0215	-0.6557	-0.2566	0.1213	0.0503	8.66
9/24/91	2	0.6386	0.1456	-0.6525	-0.3725	0.0710	0.0372	8.03
7/24/92	2	0.2312	0.1932	-0.2013	-0.3763	-0.7133	-0.4671	9.82
8/09/92	2	0.6723	0.2232	-0.6181	-0.3267	0.0913	0.0326	8.74
8/23/91	3	0.0277	-0.3395	0.0679	0.3234	0.8270	0.3015	3.26
9/24/91	3	-0.1095	0.3122	0.0161	-0.2872	-0.7960	-0.4172	2.92
7/24/92	3	0.6194	-0.2352	-0.6870	-0.0396	0.2624	0.1365	2.92
8/09/92	3	-0.0159	0.2378	0.1037	-0.3320	-0.7962	-0.4340	5.00
8/23/91	4	0.4092	-0.7486	0.2483	0.2129	-0.4013	-0.0642	2.08
9/24/91	4	0.4790	-0.6814	0.0639	0.3552	-0.4071	-0.1010	1.26
7/24/92	4	-0.0718	0.0670	-0.0536	0.0500	0.5322	-0.8377	1.45
8/09/92	4	-0.5433	0.7164	-0.1317	-0.2913	0.2903	0.0716	1.26
8/23/91	5	0.0433	-0.1329	0.1681	-0.3174	0.3635	-0.8482	1.08
9/24/91	5	-0.0527	0.1008	-0.0423	0.0300	-0.4328	0.8928	0.82
7/24/92	5	0.3113	-0.7373	-.3810	0.3288	-0.2265	-0.2342	1.22
8/09/92	5	0.0743	-0.2756	0.4376	-0.7928	0.1552	0.2727	0.58
8/23/91	6	0.0104	-0.1712	0.3651	-0.8071	0.0593	0.4271	0.95
9/24/91	6	0.0853	-0.3674	0.4658	-0.7870	0.0700	0.1289	0.65
7/24/92	6	-0.1174	0.2489	-0.3574	0.8474	-0.2715	-0.0691	0.87
8/09/92	6	0.0358	-0.1146	0.0824	-0.1097	0.4871	-0.8541	0.28

Table B-1. PC eigenvectors and percent of total variation for four Lake Mead

Band Ratios

Band ratios are sometimes used to determine chlorophyll-a concentrations in turbid waters (Lathrop et al., 1991, Stumpf and Tyler, 1988). The reason for using ratios is that they are unaffected by the amplitude of the reflectance of a water body and instead measure differences in water color. In waters containing varying concentrations of suspended mineral sediment, color differences can often be related to chlorophyll concentration, while single band reflectances cannot (Stumpf and Tyler, 1988). The most successful band ratios involve a wavelength that is sensitive to algal light scattering (e.g. near-IR light), and another that is sensitive to pigment absorption (e.g. red light). Increased chlorophyll will reduce red light reflectance relative to near-IR reflectance. The near-IR band thereby effectively normalizes the ratio for turbidity changes.

Ratios only compensate for those factors which operate equally across the bands and which are not additive in nature; i.e., the factors must cancel in interband division (Lathrop et al., 1991). Atmospheric path radiance and clear water reflectance are additive terms that cannot be removed via ratioing. It is therefore necessary to remove these factors prior to ratioing. For water bodies with significant areas of clear water, the magnitude of scene path radiance and clear water reflectance is estimated for

each band as the darkest pixel falling within the water body. When using TM data, this value is taken from the debanded, averaged imagery. This "dark pixel subtraction" technique assumes a laterally homogeneous atmosphere, which is usually a reasonable assumption for lakes within a single TM image.

TM grey values can be converted to radiance values prior to ratioing using the calibrations factors provided with each TM scene. This conversion is recommended if ratios are to be compared between different sensors, or over long time periods. But for single date analyses, this conversion is superfluous. Ratios generated from dark-pixel-corrected TM grey values are exactly and linearly related to ratios generated from dark-pixel-corrected radiance values because TM grey values are linearly related to radiance.

Despite their ability to accurately map chlorophyll-a concentrations under certain conditions, ratios of images from broad-band sensors like TM are not a panacea for mapping chlorophyll-a concentration. There are several important limitations on their use:

- Ratios are not useful for mapping chlorophyll-a in clear water (reflectance less than 0.01) (Stumpf and Tyler, 1988).
  As the denominator of the ratio approaches that of clear water radiance, ratio values become very unstable and susceptible to image noise.
- Relationships between ratio values and chlorophyll-a will change with different algal species.
  Differences in pigment concentrations and cell wall reflectance between species affect ratio values.
- Differing suspended sediment compositions affect ratio values.
- Ratios cannot remove the effect of sun glint.
  Sun glint is additive in nature and therefore is not removed by ratioing. Areas of sun glint produce anomalous ratio values.

In spite of their limitations, ratios of TM data can be used to map chlorophyll-a concentration in many cases. Differing water bodies contain various mixtures of pigments, mineral sediments, and dissolved chemicals which will change the relationship between ratio values and chlorophyll-a concentration. The optimal bands for use in a ratio will depend on these local environmental conditions.

TM4/TM3 and TM3/TM1 ratios were examined for the 10/14/92 Lake Powell TM scene. Results of regression models which use these ratios to predict chlorophyll-a were compared to those that use raw TM data. In all cases, the ratios never produced better results than the raw data, even if samples were stratified so that only pixels from turbid water (Secchi depth <= 6m) were included in the data set. In most cases, the ratios yielded far worse results. Therefore, ratios were rejected in favor of the de-banded, averaged TM data.

LITERATURE CITED

Anuta, P. E., L. A. Bartolucci, M. E. Dean, D. F. Lozano, E. Malaret, C. D. McGillern, J. A. Valdes, and C. R. Valenzuela, 1984. Landsat-4 MSS and Thematic Mapper data quality and information content analysis, *IEEE Transactions on Geoscience and Remote Sensing*, Vol. GE-22, No. 3, 222-236.

Barker, J. L., 1985. Relative radiometric calibration of Landsat TM reflective bands, *Proceedings of the Landsat-4 Science Characterization Early Results Symposium*, Greenbelt, Maryland, 22-24 February 1983, NASA Conference Publication 2355, Vol. 3, 1-219.

Bartolucci, L. A. and M. Chang, 1988. Look-up tables to convert Landsat TM thermal IR data to water surface temperatures, *Geocarto International*, Vol. 3, 61-67.

Brush, R. J. H., 1993. Anomalous effects of sunglint on the AVHRR in the NOAA-12 satellite, *International Journal of Remote Sensing*, Vol. 14, No. 4, 629-634.

Crippen, R. E., 1989. A simple spatial filter routine for the cosmetic removal of scan-line noise from Landsat TM P-tape imagery, *Photogrammetric Engineering and Remote Sensing*, Vol. 55, No. 3, 327-331.

Chahine, M. T., D. J. McCleese, P. W. Rosenkranz, and D. H. Staelin, 1983. Interaction mechanisms within the atmosphere, in *Manual of Remote Sensing*, Vol. 1, edited by R. N. Colwell, D. S. Simonett and F. T. Ulaby, pp. 176-230. Falls Church, VA: American Society of Photogrammetry.

Cole, G. A., 1979. *Textbook of Limnology*, 2nd Edition. Saint Louis: Mosby.

Dekker, A. G., T. J. Malthus, M. M. Wijnen, and E. Seyhan, 1992. The effect of spectral bandwidth and positioning on the spectral signature analysis of inland waters, *Remote Sensing of Environment*, Vol. 41, 211-225.

Dierberg, F., 1992. *Remote Sensing for Water Quality Monitoring in the Tennessee Valley - Field Tests of Two Systems*, TVA/WR-92/17, Tennessee Valley Authority, Water Resources Division, Chattanooga, TN. 123 pp.

Helder, D. L., B. K. Quirk, and J. I. Hood, 1992. A technique for the reduction of banding in Landsat Thematic Mapper images, *Photogrammetric Engineering and Remote Sensing*, Vol. 58, No. 10, 1425-1431.

Khorram, S., 1985, Development of water quality models applicable throughout the entire San Francisco Bay and Delta, *Photogrammetric Engineering and Remote Sensing*, Vol. 51, No. 1, 53-62.

Langley, Richard B., 1991. The mathematics of GPS, *GPS World*, Vol. 2, No. 7, 45-50.

Lathrop, R. G. and T. M. Lillesand, 1986. Use of Thematic Mapper data to assess water quality in Green Bay and Central Lake Michigan, *Photogrammetric Engineering and Remote Sensing*, Vol. 52, No. 5, 671-680.

Lathrop, R. G. and T. M. Lillesand, 1987. Calibration of Thematic Mapper thermal data for water surface temperature mapping: case study on the Great Lakes, *Remote Sensing of Environment*, Vol. 22, No. 2, 297-307.

Lathrop, R. G., T. M. Lillesand, and B. S. Yandell, 1991. Testing the utility of simple multi-date Thematic Mapper calibration algorithms for monitoring turbid inland waters, *International Journal of Remote Sensing*, Vol. 12, No. 10, 2045-2063.

Lillesand, T. M. and R. W. Kiefer, 1987, *Remote Sensing and Image Interpretation*, Second Edition. New York: John Wiley and Sons.

Lindell, T., B. Karlsson, M. Rosengren, and T. Alfoldi, 1986. A further development of the chromaticity technique for satellite mapping of suspended sediment load, *Photogrammetric Engineering and Remote Sensing*, Vol. 52, No. 9, 1521-1529.

Lira, J., G. R. Marzolf, A. Marocchi, and B. Naugle, 1992. A probabilistic model to study spatial variations of primary productivity in river impoundments, *Ecological Applications*, Vol. 2, No. 1, 86-94.

Malaret, E., L. A. Bartolucci, D. F. Lozano, P. E. Anuta, and C. D. McGillern, 1985. Landsat-4 and Landsat-5 Thematic Mapper data quality analysis, *Photogrammetric Engineering and Remote Sensing*, Vol. 51, No. 9, 1407-1416.

Potter, L. D. and C. L. Drake, 1989. *Lake Powell: Virgin Flow to Dynamo*. Albuquerque: University of New Mexico Press.

Quibell, G., 1992. Estimating chlorophyll concentration using upwelling radiance from different freshwater algal genera, *International Journal of Remote Sensing*, Vol. 13, No. 14, 2611-2621.

ReMillard, M. D., L. R. Herbert, G. a. Birdwell, and T. K. Lockner, 1992. *Water Resources Data - Utah: Water Year 1992*, U.S. Geological Survey Water-Data Report UT-92-1.

Ritchie, J. C., C. M. Cooper, and F. R. Schiebe, 1990. Relationship of MSS and TM digital data with suspended sediments, chlorophyll, and temperature in Moon Lake, Mississippi, *Remote Sensing of Environment*, Vol. 33, No. 2, 137-148.

Stockton, C. W. and G. C. Jacoby, 1976. *Long-term Surface-water Supply and Streamflow Trends in the Upper Colorado River Basin*, Lake Powell Research Project Bulletin, Number 18.

Strickland, J. D. H. and T. R. Parsons, 1968. *Practical Handbook of Seawater Analysis*, Fisheries Research Board of Canada, Bulletin 167.

Stumpf, R. P. and M. A. Tyler, 1988. Satellite detection of bloom and pigment distributions in estuaries, *Remote Sensing of Environment*, Vol. 24, 385-404.

U.S. Bureau of Reclamation, 1990. *Bureau of Reclamation Power Facilities: Hydroelectric Powerplants for which the Bureau of Reclamation has Operating Responsibility - Fiscal Year 1990*.

Verdin, J. and D. Wegner. 1984. Application of multispectral digital imagery to the assessment of primary productivity in Flaming Gorge Reservoir. Pages 63-68 in Proceedings of the third Annual Conference of the North American Lake Management Society, Knoxville, *Lake and reservoir management*. Washington, D.C.: EPA, Office of Water Regulations and Standards.

Wen-yao, L. and V. Klemas, 1988. Quantitative analysis of distribution of suspended sediments in the Yellow River estuary from MSS data, *Geocarto International*, Vol. 1, 51-62.